

Automatic Design of Missions to Small Bodies

Javier Roa,* Alan B. Chamberlin,† Ryan S. Park,‡ Anastassios E. Petropoulos,§ Paul W. Chodas,¶ Damon Landau,||
Davide Farnocchia**

Jet Propulsion Laboratory, California Institute of Technology, Pasadena, CA, 91109, USA

The new JPL Small-Body Automatic Mission-Design System comprises two main elements: a database of pre-computed mission options to all known asteroids and comets, and an interactive web interface that can be used to design transfers to each small body. The system is kept current with the JPL Small Body orbit catalog, is publicly available, and can be accessed from the JPL Solar System Dynamics Group website. The missions computed by the automatic system are impulsive. However, a low-thrust Δv estimate is also provided. The database of pre-computed missions can be filtered to find potential targets with certain orbital and physical properties, and that meet specific mission-design constraints. In addition to describing the system in detail, this paper presents empirical analytic expressions to approximate the impulsive Δv requirements of missions to comets and to each family of asteroids, obtained by fitting statistical data. To show how the interactive interface works, we consider mission options to asteroid 99942 Apophis. We also include optimal mission opportunities to other selected small bodies.

I. Nomenclature

a	=	semimajor axis
C_3	=	characteristic energy of launch, v_∞^2
d	=	MOID
e	=	eccentricity
P	=	orbital period
q	=	perihelion distance
Q	=	aphelion distance
T	=	Tisserand parameter (nondimensional)
v_∞	=	hyperbolic excess velocity
μ	=	gravitational parameter (GM) of the Sun
DLA	=	declination of the launch asymptote
MOID	=	minimum orbit intersection distance
SEP angle	=	Sun-Earth-Probe angle (solar elongation)

II. Introduction

SMALL bodies (asteroids and comets) are scientifically interesting because they can provide valuable information about the origin and evolution mechanisms of the Solar System. Their composition, shape, internal structure, orbital regime, etc. are the result of thousands of years of evolution, subject to complex physical processes. Moreover, near-Earth objects can potentially impact Earth, so they must be constantly monitored in order to predict the collision probability. Asteroids and comets are divided into families depending on their orbital regimes. Table 1 presents the orbital distribution of small bodies by family.

*Postdoctoral Scholar, Solar System Dynamics Group. Member AIAA.

†Navigation Engineer, Solar System Dynamics Group.

‡Group Supervisor, Solar System Dynamics Group.

§Mission Design Engineer, Outer Planets Mission Analysis Group.

¶Manager, Center for Near-Earth Object Studies.

||Mission Design Engineer, Mission Concept Systems Development Group

**Navigation Engineer, Solar System Dynamics Group.

Table 1 Small-body population by July 2017

Family	Code	Definition	Number of objects	Fraction
Atira	IEO	$Q < 0.983$ au	16	< 0.01%
Aten	ATE	$Q > 0.983$ au; $a < 1$ au	1,199	0.16%
Apollo	APO	$a > 1$ au; $q < 1.017$ au	8,862	1.21%
Amor	AMO	1.017 au $< q < 1.3$ au	6,230	0.85%
Mars-crossing Ast.	MCA	1.3 au $< q < 1.666$ au; $a < 3.2$ au	15,524	2.11%
Inner Main-belt Ast.	IMB	$a < 2$ au; $q > 1.666$ au	14,144	1.93%
Main-belt Ast.	MBA	2 au $< a < 3.2$ au; $q > 1.666$ au	656,967	89.44%
Outer Main-belt Ast.	OMB	3.2 au $< a < 4.6$ au	22,075	3.01%
Jupiter Trojan	TJN	4.6 au $< a < 5.5$ au; $e < 0.3$	6,668	0.91%
Centaur	CEN	5.5 au $< a < 30.1$ au	407	0.06%
Trans-Neptunian Objects	TNO	$a > 30.1$ au	2,350	0.32%
Other	–	–	102	0.01%
Total Asteroids			734,544	100%
Hyperbolic Comet	HYP	$e > 1$ (typically $e - 1 \ll 1$)	331	9.52%
Parabolic Comet	PAR	$e = 1$	1,838	52.86%
Jupiter-family Comet	JFc	$P < 20$ yr or $2 < T_{\text{Jup}} < 3$	656	18.87%
Halley-type Comet	HTc	20 yr $< P < 200$ yr	73	2.10%
Encke-type Comet	ETc	$T_{\text{Jup}} > 3$; $a < a_{\text{Jup}}$	48	1.38%
Chiron-type Comet	CTc	$T_{\text{Jup}} > 3$; $a > a_{\text{Jup}}$	13	0.37%
Other	–	–	518	14.90%
Total Comets			3,477	100%

Although several space missions have already explored asteroids and comets, like Dawn, Rosetta, Hayabusa, NEAR, and Giotto, small bodies still pose unique challenges for mission designers due to their diverse dynamics. One of the main difficulties is selecting the best target for scientific exploration in such vast population subject to mission-design constraints. As of July 2017, there were 738,021 small bodies whose orbits had been determined. In addition, new discoveries are frequent, and the catalog keeps evolving. Any process that aims to process small bodies needs to be automated in order to keep track of the current population and manage new discoveries.

To automatically keep track of the entire catalog of known small bodies, the Solar System Dynamics Group at the Jet Propulsion Laboratory (JPL) developed an automatic orbit-determination system. The system is updated, as new observations become available, to refine the computed orbit solutions. This automatic system has been providing accurate orbits of asteroids and comets for more than 20 years.

The goal of the present project is to develop a new automatic mission-design system that will complement the orbit-determination system described above. Following the same philosophy, the new system computes mission options to each known asteroid and comet. All of the pre-computed solutions will then be available to the user for filtering and further post-processing. In addition to processing a set of candidate missions, users can also design new missions thanks to a new web interface for interactive mission design. The mission-design system always works with the latest high-fidelity orbit solution available, meaning that the user does not have to deal with generating the ephemeris of the small bodies. Section III is devoted to explaining the architecture and components of the system. The system constantly updates the database of mission opportunities and the web interface is connected to a back-end process that uses the latest orbit solution, so all data is kept up-to-date automatically.

With more than 200 million trajectories at hand, Sec. IV analyzes the requirements of missions to small bodies from a statistical perspective, organized by families. We found empirical formulae that provide a good analytic approximation of the C_3 requirements when fitted to the mission-design data. Finally, Sec. V shows how the interactive web interface

works, focusing on the design of future missions to the near-Earth asteroid 99942 Apophis as an example.

Dedicated surveys of mission opportunities to certain asteroid families can be found in the literature. Near-Earth asteroids (NEA) have been studied in detail, since their proximity to Earth reduces the launch requirements. Back in the late 1970s, an early study by Shoemaker and Helin [1] explored the feasibility of missions to near-Earth asteroids motivated by the scientific information that such missions can provide about the formation of the asteroid main belt. More recently, sending humans to asteroids has been considered as a stepping stone in the preparation of hypothetical crewed missions to Mars. Human missions require heavier spacecraft and relatively short times of flight, which originated several studies considering different propulsion systems and mission architectures [2–4]. The Center for NEO Studies at JPL (CNEOS) hosts the NHATS system, which finds round-trip opportunities to near-Earth objects automatically [5]. An interesting study of rendezvous strategies to NEA can be found in Ref. [6].

III. The JPL Small-Body Automatic Mission-Design System

The goal of the new JPL Small-Body Automatic Mission-Design System is to enable rapid selection of potential targets for future scientific missions, and to support preliminary mission-design analyses to asteroids and comets. The system will be publicly available and can be accessed online from the JPL Solar System Dynamics Group website, <https://ssd.jpl.nasa.gov/mdesign>. The system front-end includes two main elements:

- **Database of pre-computed solutions:** mission options to each small body in the Small-Body Database are computed periodically, and the most promising opportunities are stored in the database. The database can then be filtered to obtain lists of small bodies that satisfy certain constraints. Using the [Small-Body Search Engine](#), it is now possible to filter objects not only by physical parameters (magnitude, diameter, albedo, etc) and orbital parameters (semimajor axis, eccentricity, inclination, etc), but also by mission-design parameters (see Table 2 for a description of the available parameters). Combining constraints on different parameters, this tool can be used for identifying potential missions that are both scientifically relevant and feasible.
- **Interactive web interface:** each asteroid and comet can be analyzed in more detail using an interactive web interface. The interface allows the user to select new mission options by simply clicking on different interactive plots. Thanks to this tool, users will no longer need to retrieve the latest ephemeris for the asteroid or comet, or keep track of recent discoveries, orbit linkages, designation changes, or lost objects.

The system updates the mission-design data every time the orbit of a small body is determined using new observations. The system propagates the orbits of asteroids and comets using the same force model used in the orbit determination process, including all of the relevant perturbations.

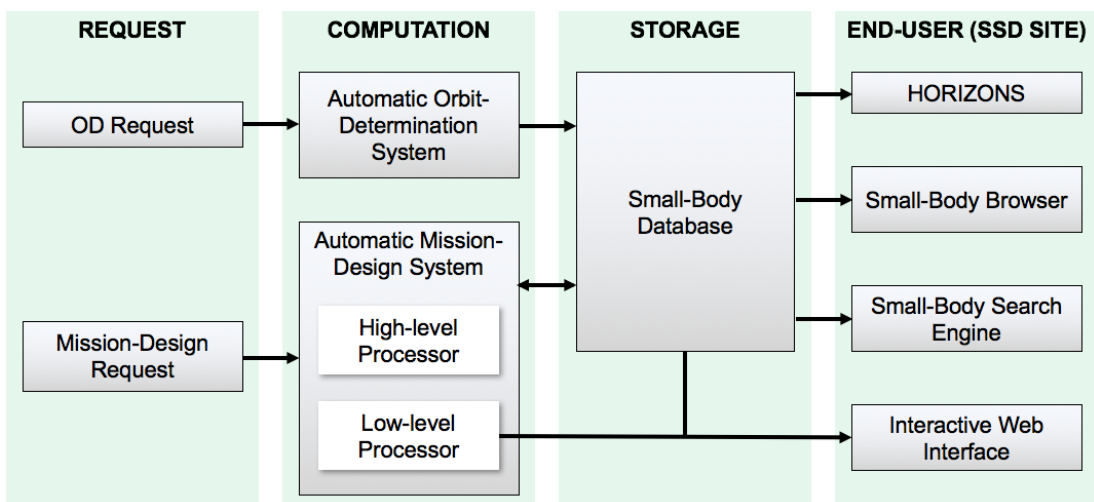


Fig. 1 Integrated architecture of the orbit-determination and mission-design systems

Figure 1 describes the architecture of the new mission-design system, integrated with the existing automatic orbit determination pipeline. Whenever a new object is discovered or new observations are available, a request for orbit determination is generated. The new observations are fit and the resulting new orbit solution is stored in the Small-Body Database. The user can then access all of the tools available in the JPL Solar System Dynamics Group website that

will use the latest orbit solution. In addition, CNEOS provides specific tools for the analysis of near-Earth objects.* Once the new orbit solution is available, the automatic mission-design system will process the object. First, a high-level processor receives the request and retrieves the orbit solution from the database. Second, the low-level core carries out the computations described in Sec. A, generating a list of mission options. The subset of pre-computed solutions is then pushed into the database, which can be accessed from the public website using the Small-Body Search Engine. Finally, the interactive interface not only retrieves the list of pre-computed solutions, but also interacts directly with the low-level core to get the high-resolution pork-chop plot (see Sec. B for more details).

All pre-computed missions are impulsive, assuming the launch vehicle provides an adequate v_∞ to depart from Earth and reach the target. In addition, we provide an estimate of the Δv required for a phase-free, low-thrust transfer with constant thrust acceleration [7].

A. Automatic Mission Selection

The core of the system is the automatic selection of optimal mission opportunities. For this purpose, we developed a feature-extraction algorithm based on two layers of optimization. Each “mission” is defined by the set of parameters in Table 2.

Table 2 Parameters defining each pre-computed mission stored in the database

Parameter	Description
Designation	Primary designation of the small body.
Departure date	Date of departure from Earth.
Arrival date	Date of arrival at the small body.
Departure v_∞	Required hyperbolic excess velocity upon departing from Earth.
Arrival v_∞	Hyperbolic excess velocity upon arrival at the small body.
Phase angle	Sun phase angle, formed by the incoming v_∞ -vector and the Sun-target vector.
Range	Distance to Earth at arrival.
DLA angle	Declination of the launch asymptote, angle between the outgoing v_∞ -vector and the Earth equator.
SEP angle	Sun-Earth-Probe angle (solar elongation) at arrival.
Pump angle	Angle between the incoming v_∞ -vector and the heliocentric velocity vector of the small body.

Given an asteroid or comet, the first step in the process is the generation of the pork-chop plot. Lambert’s problem is solved using the algorithm in Ref. [8]. The mission-data will be updated at least once a year, with the launch period extending 25 years into the future. The time-of-flight limits are defined using fractions of the time corresponding to a Hohmann transfer:

$$t = k\pi\sqrt{\frac{a_H^3}{\mu}}. \quad (1)$$

In this expression, k is a constant factor that can be adjusted for each orbit class. Typical values are $k = 3$ for the maximum time of flight, and $k = 1/4$ for the minimum time of flight. To capture rapid missions during close approaches, the minimum time of flight will be reduced to 10 days if the minimum orbit intersection distance (MOID) is less than 0.01 au and $q < 1.0267$ au. The semimajor axis of the Hohmann ellipse is simply

$$a_H = \frac{1}{2}(a_E + r_{\text{ref}}), \quad (2)$$

where the subscript E refers to Earth. When estimating the minimum time of flight, r_{ref} is the perihelion distance, and we set r_{ref} equal to the aphelion distance when estimating the maximum time of flight. For the case of open orbits, instead of the perihelion and aphelion distances, we use the closest and furthest points from Earth’s orbit in the 25-year launch period. We set a time resolution of 5 days.

Once the transfer map is computed, a global search (first layer) is conducted using a sliding window in order to find locally optimal launch opportunities. There are two criteria for selecting optimal launch windows. First, the algorithm

*<https://cneos.jpl.nasa.gov>

selects those launch dates that minimize the departure v_∞ in the 25-year launch span. Second, the launch dates for which the arrival v_∞ is minimized are selected too, as long as that particular mission option is not too close in time to an already selected mission, and $C_3 < 150 \text{ km}^2/\text{s}^2$ at departure.

The second layer of the feature-extraction algorithm seeks mission opportunities that minimize or maximize other mission-design parameters, under certain C_3 constraints. Starting from each solution found within the first layer, the search algorithm looks for local minima of the time of flight, total Δv (sum of departure and arrival v_∞), phase angle, pump angle, range, and departure date. In addition, it looks for local maxima of the DLA and the SEP angles, to sample as many distinctive features as possible. The second layer will run several times, with different C_3 limits, both absolute and relative to the local minima from which the local search started. Finally, the search algorithm selects the minimum and maximum departure and arrival dates for each launch window. Figure 2 shows a launch window to asteroid 3 Juno, and the blue dots correspond to the missions selected by the feature-extraction algorithm. Note how the minimum departure C_3 as well as various minimum-time solutions are captured. Additional solutions, like the earliest/latest departure/arrival cases, are selected too. The annotations explain the reason why the feature-extraction algorithm chose certain missions in that particular example.

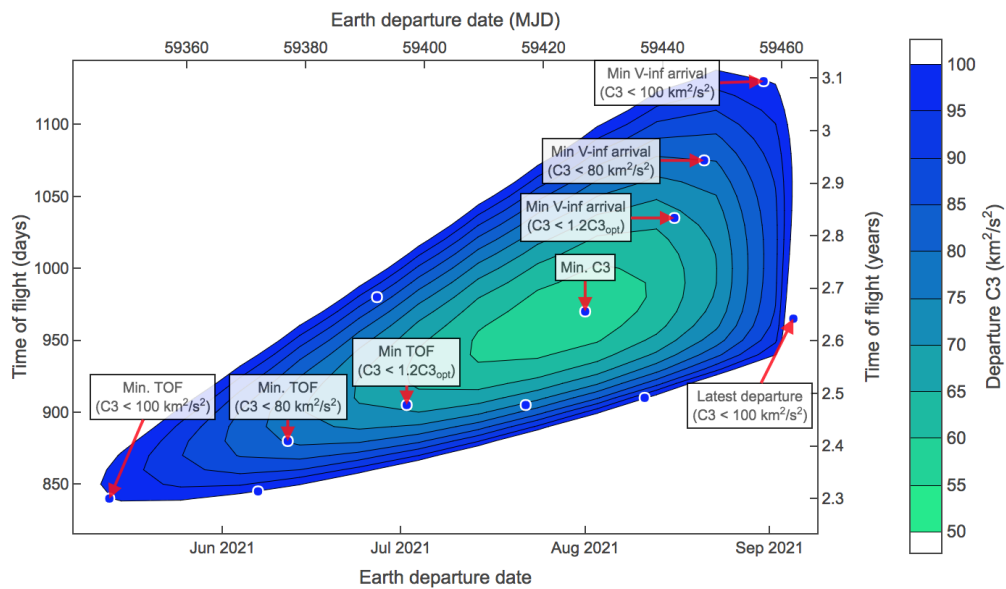


Fig. 2 Missions selected by the feature-extraction algorithm for an example launch window (asteroid 3 Juno)

Every time the system processes a small body, all of the solutions already in the database for that particular object are deleted before pushing the new set of missions. The configuration parameters for the feature extraction have been tuned in order to capture the most representative features of the map with the minimum number of points possible.

B. Interactive Web Interface

The goal of the interactive interface is to allow users to select mission options to any small body, different from the ones that were pre-computed automatically and stored in the database. Thanks to this extra flexibility, the interface can potentially be used in preliminary studies for many kinds of missions. The interface comprises three main elements:

- 1) **Table of selected missions:** initially, this data table is populated with all pre-computed missions found in the database generated by the procedure described in A. Apart from the parameters listed in Table 2, the table presents the time of flight, the departure C_3 , and the capabilities of different launch vehicles considering both flyby and rendezvous missions. Additional solutions selected by the user with the tools described below will be added to this table. The table can be downloaded for post-processing or archiving.
- 2) **Interactive pork-chop plot:** a pork-chop plot is generated in real time, displaying contours for two parameters at the same time. By default, the system plots the departure C_3 and the arrival v_∞ , but the user can choose any of the mission-design parameters in Table 2, as well as the total Δv or the rendezvous mass with different launch vehicles. The data can be easily explored by hovering the mouse over the figure. Clicking on any point of the plot adds the corresponding transfer opportunity to the table of selected missions.

- 3) **Launch-vehicle selection tool:** this tool compares the performance of different launch vehicles in a given range of launch dates. It shows the maximum mass that can be delivered to the target for flyby/rendezvous missions as a function of the launch date. The user can easily choose launch dates and add the corresponding missions to the data table.

Section V uses the 2029 close approach of asteroid 99942 Apophis as an example to show how the interactive interface works. Each interactive design tool will be explained in more detail.

IV. Feasibility Analysis

The new mission-design database includes, on average, around 300 transfer options to each small body. But the actual number of feasible missions varies significantly depending on the orbit class, and even within the same family of objects. In this study, we consider a mission to be feasible if the required departure C_3 from Earth is less than $150 \text{ km}^2/\text{s}^2$. This upper bound comes from the limitations of current launch vehicles and upper stages. We also set a maximum time of flight of 40 years, although it is hardly ever reached because the limit in Eq. (1) is more restrictive.

Figure 3 shows the distribution of the minimum departure C_3 across the different families of asteroids, from 2017 to 2042. Table 6 in the Appendix lists optimal mission options for targeting each family. Identifying the optimal launch opportunity is a form of assessing the feasibility of missions to a certain target body, as well as the minimum requirements for orbit transfers. Due to their proximity to Earth’s orbit, near-Earth asteroids (NEA) require lower departure C_3 than other families of asteroids. More than 85% of the asteroids in this family can be reached with $C_3 \leq 6 \text{ km}^2/\text{s}^2$, which is equivalent to a departure v_∞ of less than 2.4 km/s. Falcon 9, a popular launch vehicle for low-Earth orbiting satellites with a C_3 limit[†] around $10 \text{ km}^2/\text{s}^2$, could potentially reach 90% of the entire NEA population. More than 98% of all NEA could be reached by Antares-class rockets, and heavier launchers like Atlas V or Delta IV Heavy will allow missions to virtually all NEA.

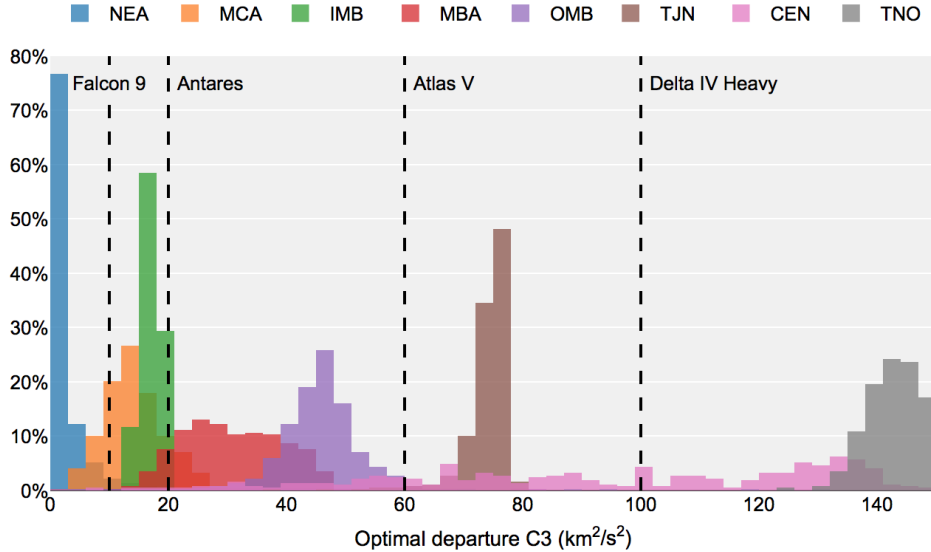


Fig. 3 Distribution of optimal departure C_3 for all reachable asteroids organized by families (bins are $3 \text{ km}^2/\text{s}^2$ in size)

Among Mars-crossing asteroids (MCA), the most likely optimal C_3 value is around $13 \text{ km}^2/\text{s}^2$. Launch vehicles achieving up to $C_3 = 20 \text{ km}^2/\text{s}^2$ will reach 95% of MCA. When dealing with quasi-circular orbits, the main factor driving the required departure energy is the semimajor axis of the orbit. This phenomenon is the reason why the families of inner and outer main-belt asteroids (IMB and OMB, respectively) flank the actual set of main-belt asteroids (MBA); for IMB the most likely optimal C_3 value is close to $17 \text{ km}^2/\text{s}^2$, for OMB it is $47 \text{ km}^2/\text{s}^2$, and over 99% of MBA fall within this range.

There is a clear gap between OMB and Jupiter Trojans (TJN). The semimajor axis of the latter family goes up to 5.5 au, and the optimal departure C_3 for most TJN is at least $74 \text{ km}^2/\text{s}^2$. Trans-Neptunian objects (TNO) are hard to

[†]elvperf.ksc.nasa.gov

reach with direct transfer missions, with the required C_3 amounting to over $140 \text{ km}^2/\text{s}^2$. Missions to this type of asteroids will most likely require intermediate gravity-assist maneuvers, or low-thrust propulsion systems. Nevertheless, feasible direct missions to 585 TNO have been found. Centaurs (CEN) present a special behavior: due to their high eccentricity (up to 0.94), the minimum C_3 required to reach asteroids in this family ranges from $6 \text{ km}^2/\text{s}^2$ to more than $140 \text{ km}^2/\text{s}^2$.

What remains of the section is devoted to characterizing each asteroid family separately, and reachable comets are also discussed. Approximate analytic expressions for the launch requirements are derived from the data.

A. Accessible NEA

Near-Earth asteroids are particularly interesting from a mission-design perspective, as their proximity to Earth brings down the departure v_∞ required to reach them. The mission requirements are strongly correlated with the MOID between the orbit of the asteroid and the orbit of the Earth. Intuitively, the smaller the MOID the lower the outgoing v_∞ from Earth will be, as shown in Fig. 4. The figure shows the distribution of asteroids by their MOID with respect to Earth and the minimum v_∞ required to reach them.

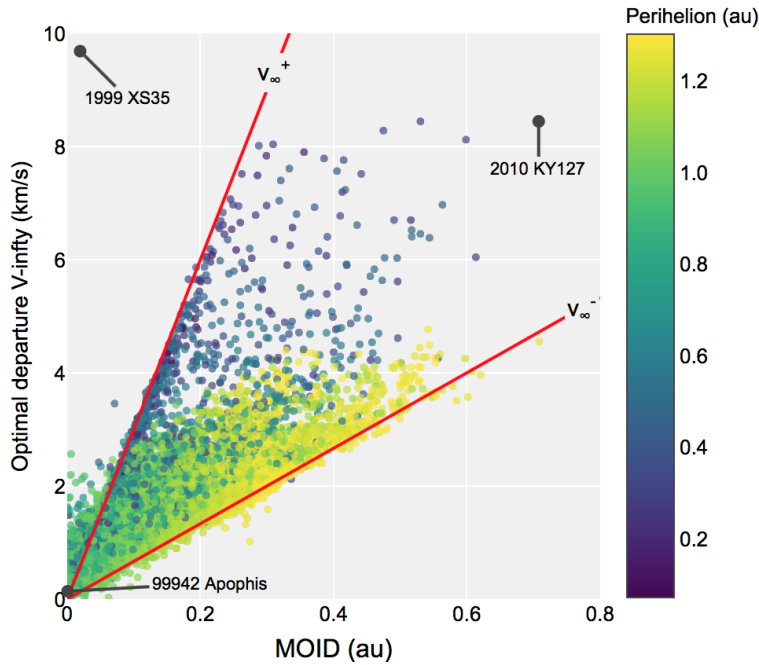


Fig. 4 Distribution of near-Earth asteroids (NEA) by MOID and departure v_∞

The distribution of asteroids forms a clear triangular pattern, with upper and lower bounds on the departure v_∞ that can be approximated by two linear functions of the MOID d :

$$\begin{aligned} v_\infty^+(d) &= 30d \\ v_\infty^-(d) &= 6.7d. \end{aligned} \quad (3)$$

The MOID d is defined in au, and v_∞^\pm in km/s. It should be noted that for low values of the MOID, the upper bound v_∞^+ provides a too optimistic estimate of the highest departure v_∞ . Thus, $v_\infty^+(d)$ is better approximated by:

$$v_\infty^+ = \begin{cases} 2, & \text{if } d \leq 0.06 \text{ au} \\ 30d, & \text{if } d > 0.06 \text{ au} \end{cases} \quad (4)$$

The color scale indicates the perihelion distance of each asteroid. The distribution observed in Fig. 4 suggests that, for the same MOID, asteroids with perihelion closer to 1 au will exhibit lower optimal v_∞ values. This behavior was expected, because NEAs with Earth-like orbits have low eccentricity and $a \sim 1$ au, so they are easier to reach.

Asteroid 1999 XS₃₅ is a clear outlier; although its MOID is less than 0.02 au, the minimum required v_∞ is almost 10 km/s. The reason is that this asteroid has the longest orbital period of all reachable NEA, 75.2 years ($a = 17.8$ au). Its

next close approach to Earth will be in late 2075. Therefore, the only way to reach this object with the current mission constraints ($C_3 < 150 \text{ km}^2/\text{s}^2$ and launch before 2043) is to insert the spacecraft in a very wide, eccentric orbit in late 2042 that comes back 33 years later to reach the asteroid at its time of closest approach to Earth. Asteroid 2010 KY₁₂₇ has the highest MOID, 0.71 au and is an interesting example of a mission to a highly inclined target ($i = 60.8 \text{ deg}$), in which the optimal transfer is close to a Homann transfer contained in the ecliptic plane. Asteroid 99942 Apophis, relevant due to its close approach to Earth in October 2029, falls close to the origin of the plot.

B. Accessible Mars-Crossing Asteroids

Mars-crossing asteroids (MCA) get as close as 0.3 au to the orbit of the Earth, with $q > 1.3 \text{ au}$. This property, together with the fact that MCA orbits have lower eccentricities and inclinations than NEA, results in a more compact distribution when correlating the departure v_∞ with the MOID. Figure 5 shows that MCAs are confined to a lentic-shaped region in (v_∞, d) space, which can be approximately bounded by the functions $v_\infty^+(d)$ and $v_\infty^-(d)$. We propose the empirical formula

$$v_\infty(d) = c_1 \log(c_2 d^2 + c_3 d + c_4), \quad (5)$$

where d is in au and v_∞ in km/s. This expression is written in terms of four coefficients c_i to be fitted from data. For similar values of the MOID, only the asteroids with the highest and lowest v_∞ are used in the fit, and outliers are removed manually. For this particular family, the best-fit coefficients (minimum root-mean-square residuals) are given in Table 3.

Table 3 Coefficients of the logarithmic fit for Mars-crossing asteroids

	c_1	c_2	c_3	c_4
v_∞^+	0.4660	319680	-93433	1
v_∞^-	1630	0.003523	-0.000722	1.001

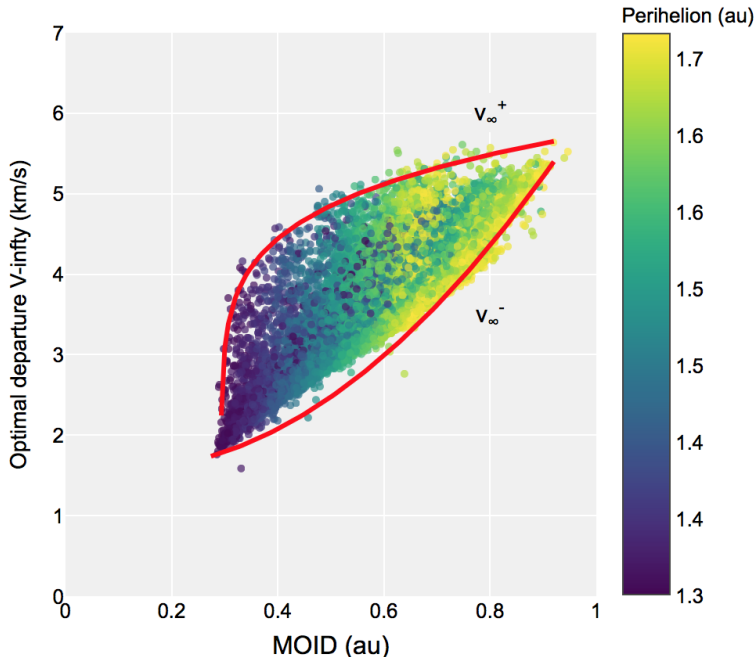


Fig. 5 Distribution of Mars-crossing asteroids (MCA) by MOID and optimal departure v_∞

The analytic approximation of the lower and upper bounds on the required departure v_∞ can be used for rapid assessments of the requirements of potential missions to MCA.

C. Accessible Main-Belt Asteroids

Main-belt asteroids (MBA) are, by far, the most common type of asteroid (almost 90% of the entire asteroid population). While the current mass of the asteroid main belt is estimated to be around 0.05% Earth masses (the four major bodies in the main belt, Ceres, Vesta, Pallas, and Hygiea are the major contributors), it is believed that the original mass was comparable to that of Earth, and that it was gradually cleared by perturbing planets [9]. Understanding the origin and evolution of the asteroid main belt is a key factor when analyzing the accretion and migration mechanisms that resulted in the Solar System that we know today.

From a mission-design point of view, MBAs form a rather homogeneous group in terms of orbital elements, with eccentricities under 0.5. Since the orbits are fairly circular, the semimajor axis is the parameter that drives the minimum C_3 requirements for reaching a given asteroid. Figure 6 shows the two-dimensional density of MBA in (C_3, a) space. The lower density of asteroids for certain values of the semimajor axis corresponds to the Kirkwood gaps, regions that were cleared due to $n : m$ mean motion resonances with Jupiter. The optimal departure C_3 histogram shows that the most likely value of the minimum required characteristic energy will be approximately $27 \text{ km}^2/\text{s}^2$. The entire population of MBA can be reached with $C_3 < 50 \text{ km}^2/\text{s}^2$, an energy level that can be provided by several launch vehicles like Delta IV Heavy, Atlas V, or Falcon Heavy. The red line in the plot shows the values of C_3 predicted by a simple co-planar Hohmann transfer from 1 au to a circular orbit of radius a . For each value of a , the density plot shows that the Hohmann approximation is in fact a conservative limit that overestimates the optimal C_3 by between 10% and 20% compared to the more likely regions.

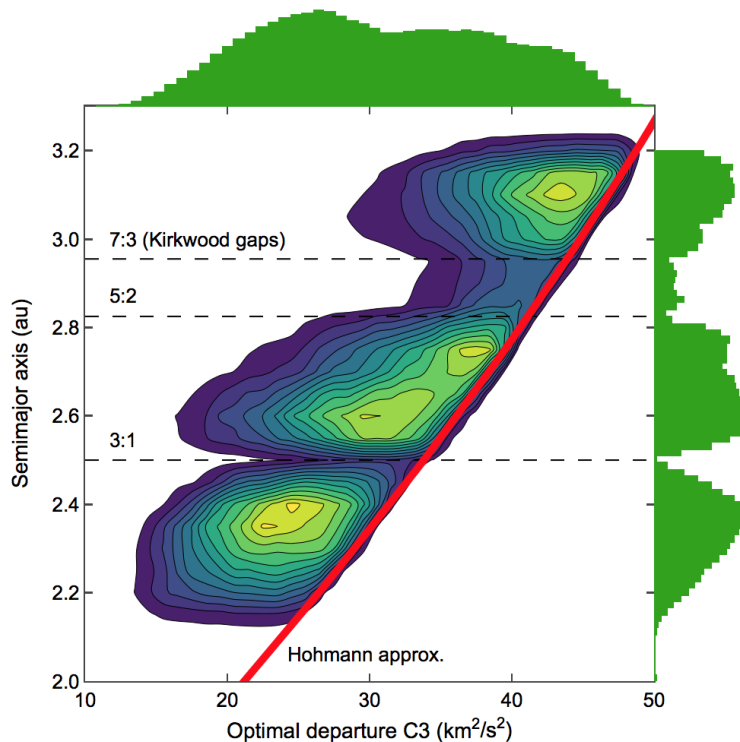


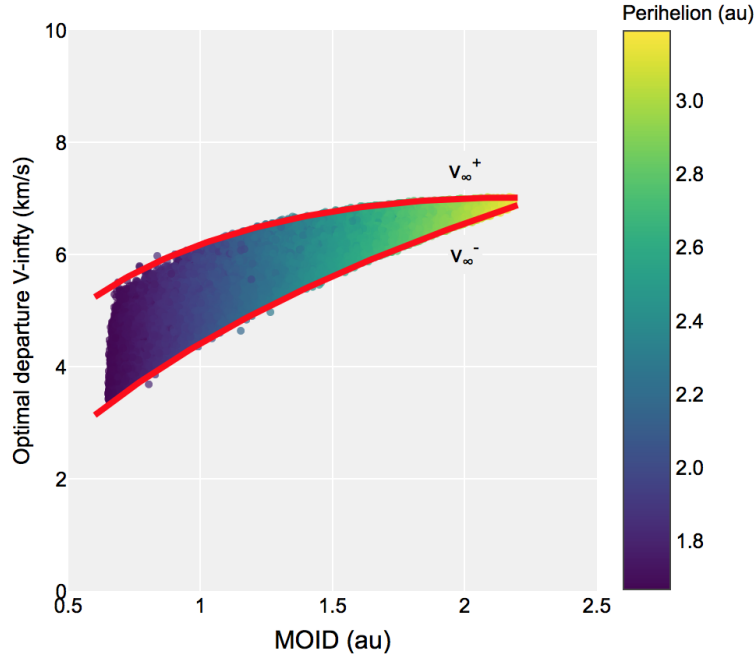
Fig. 6 Two-dimensional density distribution of main-belt asteroids by optimal required C_3 and semimajor axis

To better assess the launch requirements, Fig. 7 evaluates the dependency of the departure v_∞ on the MOID. All MBAs are confined into a well defined region that spans from $d = 0.6 \text{ au}$ to $d = 2.2 \text{ au}$. Equation (5) provides a good approximation of the lower and upper bounds of the departure v_∞ , using the coefficients in Table 4a. To accommodate inner and outer main-belt asteroids (IMB and OMB), the coefficients in Table 4b should be used in lieu of those in Table 4a.

Since the orbits of these asteroids do not cross the orbit of the Earth and their inclinations are small, the perihelion distance grows with the MOID, as seen in Fig. 7.

Table 4 Coefficients of the logarithmic fit for main-belt asteroids

	(a) MBA only				(b) MBA together with IMB and OMB			
	c_1	c_2	c_3	c_4	c_1	c_2	c_3	c_4
v_∞^+	2.677	-2.722	11.774	1	2.260	-1.539	16.199	1
v_∞^-	4.332	0	1.770	1	4.119	0	1.901	1

**Fig. 7** Distribution of main-belt asteroids by MOID and optimal departure v_∞

D. Accessible Jupiter Trojans

Jupiter Trojans (TJNs) are trapped in the Sun-Jupiter L_4 (*Greeks*) and L_5 (*Trojans*) equilibrium points, with semimajor axes between 4.6 au and 5.5 au, and $e < 0.3$. Such strict definition constrains the perihelion distance to approximately 3.2 au. The distribution of TJNs in Fig. 8 resembles the distribution of MBAs shown in Fig. 7; as the MOID increases, the difference between the lower and upper v_∞ bounds decreases, because transfers to orbits that are farther away become less sensitive to small changes in inclination or eccentricity. Several outliers have been highlighted in the figure, in particular asteroids 2011 WA₂₄, 2010 KF₉₈, and 2010 BX₁₈. It should be noted that the uncertainties in semimajor axis (1σ) for the first two asteroids are 1.14 au and 29.12 au, respectively, so mission-design results should be considered as highly uncertain too. The orbit of 2010 BX₁₈ is well determined (the 1σ uncertainty in semimajor axis is less than 0.05 au), and the reason for the high v_∞ is that the distance to Earth at arrival is 5.35 au for the optimal solution, almost 0.5 au more than the next asteroid with the same MOID.

The optimal departure v_∞ for a given MOID can be bounded using the logarithmic fit from Eq. (5) and the coefficients in Table 5. The resulting analytic expression will be valid for values of the MOID between 2.4 au and 4.4 au.

Table 5 Coefficients of the logarithmic fit for Jupiter Trojans

	c_1	c_2	c_3	c_4
v_∞^+	2.4813	14.5684	-1.4682	1
v_∞^-	3.1235	4.2812	-0.1824	1

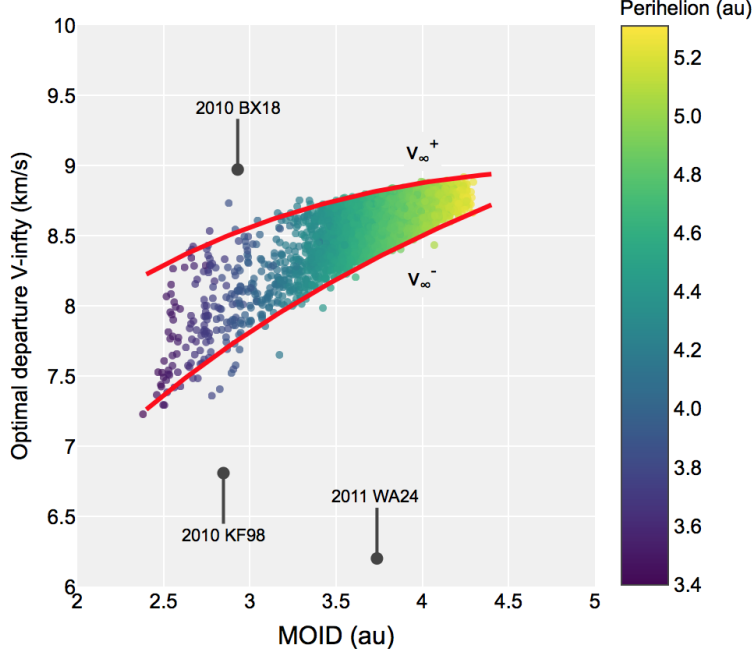


Fig. 8 Distribution of Jupiter Trojans by MOID and optimal departure v_∞

E. Accessible Centaurs

Centaurs are unique because of their unstable orbital dynamics. Horner *et al.* showed in [10] that the mean lifetime of the Centaur population is just 2.7 Myr, due to the strong perturbations from the giant planets. From a mission-design perspective, such instabilities result in a rich set of orbital regimes, with large orbits (semimajor axes between 5.5 au and 30.1 au) that are highly eccentric, highly inclined, or even retrograde. Interestingly, many Centaurs have low perihelion which brings them close to Earth, and feasible impulsive mission can be found.

Figure 9 presents the distribution of asteroids in the Centaur family that can be reached with $C_3 < 150 \text{ km}^2/\text{s}^2$ launching between 2017 and 2042. The color scale indicates the eccentricity of each orbit. Typically, low values of the MOID correspond to high eccentricities, so that the perihelion is close to or even below 1 au. On the other hand, for asteroids with similar values of the MOID, the ones with higher eccentricity most likely require higher departure v_∞ .

Asteroid 2010 LG₆₁ has the lowest launch requirements among all Centaurs, $v_\infty = 2.6 \text{ km/s}$. Its orbit is retrograde ($i = 123.7 \text{ deg}$), moderately eccentric ($e = 0.81$), and with semimajor axis $a = 7.1 \text{ au}$. However, it is highly uncertain, like the orbit of the outlier 2009 SC₂₄. Consequently, mission requirements to these objects will change as more observations are available.

We fitted the data in Fig. 9 to Eq. (5), to derive an analytic approximation of the optimal departure v_∞ as a function of the MOID. The function that minimizes the least-square residuals is

$$v_\infty(d) = 2.705 \log(-0.190d^2 + 7.484d + 1). \quad (6)$$

In this expression, the MOID d is in au and the departure v_∞ in km/s. This formula could potentially be used for rapid Δv estimates, provided that it fits most of the reachable Centaurs. For values of the MOID over 20 au, any feasible mission will require $v_\infty \gtrsim 12 \text{ km/s}$ at departure.

F. Accessible Trans-Neptunian Objects

Only 535 out of 2,350 trans-Neptunian objects (TNO) can be reached via direct launch from Earth with $C_3 < 150 \text{ km}^2/\text{s}^2$ between 2017 and 2042. The distribution of asteroids by MOID and departure C_3 in this case is homogeneous, with $v_\infty > 11 \text{ km/s}$ for all cases. The objects are so far away from Earth that the departure v_∞ is only weakly tied to the MOID, which ranges from 1.9 au (2016 PN₆₆) up to more than 45 au.

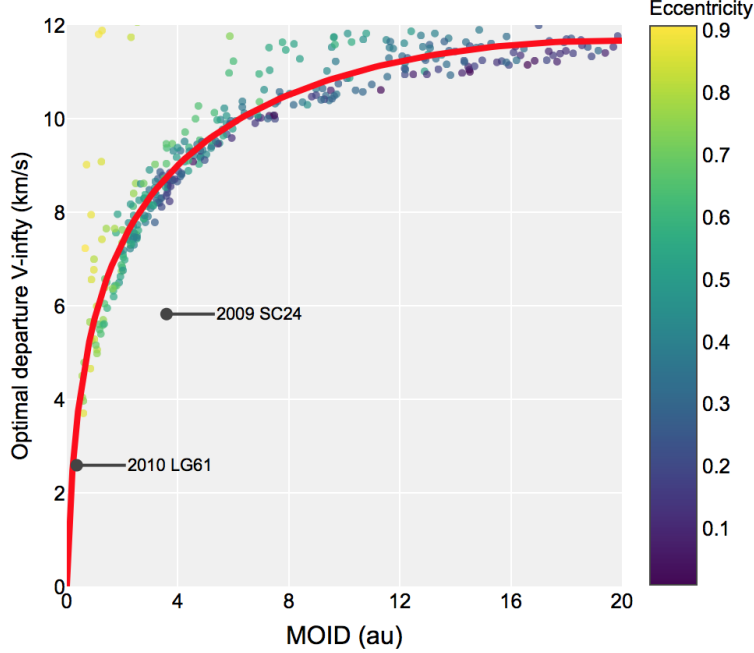


Fig. 9 Distribution of Centaurs by MOID and optimal departure v_∞

G. Accessible Comets

Comets are small bodies characterized by an icy nucleus that, due to outgassing produced by solar radiation, show distinctive cometary activity. The presence of activity is the criterion that an object needs to meet in order to be classified as comet. Although the orbits of comets typically share similar properties due to their common origin (long-period comets are thought to originate from the Oort cloud [11] and short-periods comets usually come from the Kuiper belt [12]), different dynamical regimes can be found. Their eccentricities range from $e < 0.05$ to hyperbolic cases of up to $e \approx 1.05$.

In total, we found that 737 comets can be reached via impulsive missions under the design constraints we adopted. Figure 10 summarizes the launch requirements to reach this subset of comets. The minimum v_∞ grows rapidly with the MOID, with $v_\infty > 10$ km/s for $d > 6$ au and for highly eccentric objects. It is worth pointing out that higher eccentricities typically relate to higher v_∞ for the same values of the MOID. However, comets with very low eccentricity tend to be farther away from Earth and are therefore harder to reach than comets with perihelion lower than 1 au. For this reason, we found that comets with moderate eccentricities ($e \sim 0.6$) require the lowest departure v_∞ from Earth for a given value of the MOID.

The logarithmic fit from Eq. (5) provides once more a good approximation of the v_∞ requirements:

$$v_\infty(d) = 2.9675 \log(0.0512d^2 + 4.9665d + 1). \quad (7)$$

Figure 10 also highlights the mission requirements for 9P/Tempel, 103P/Hartley, and 67P/Churyumov-Gerasimenko. These comets have been visited by the Deep Impact and the Rosetta missions, respectively. The actual departure v_∞ of the Deep Impact mission in its way to 9P/Tempel was approximately 3.4 km/s [13], and the estimate provided by Eq. (7) is 3.7 km/s.

V. Example of Preliminary Design: Close Approach of 99942 Apophis

Observations of 99942 Apophis in 2004 increased the probability of this asteroid impacting the Earth up to 2.7%. Although later observations revealed that an impact was in fact unlikely [14], during its close approach on April 13, 2029 it will pass around 32,000 km above the surface of the Earth (below geostationary orbits).

Figure 11 presents the optimal launch windows in the 2027–2032 interval. The plot has been generated using the interactive web interface. Two contours are displayed at the same time: with solid color levels from green to blue, the departure C_3 ; with contour lines from red to yellow, the arrival v_∞ . Each blue dot corresponds to a pre-computed trajectory stored in the database. It is easy to identify the time of close approach in early 2029, because as the time

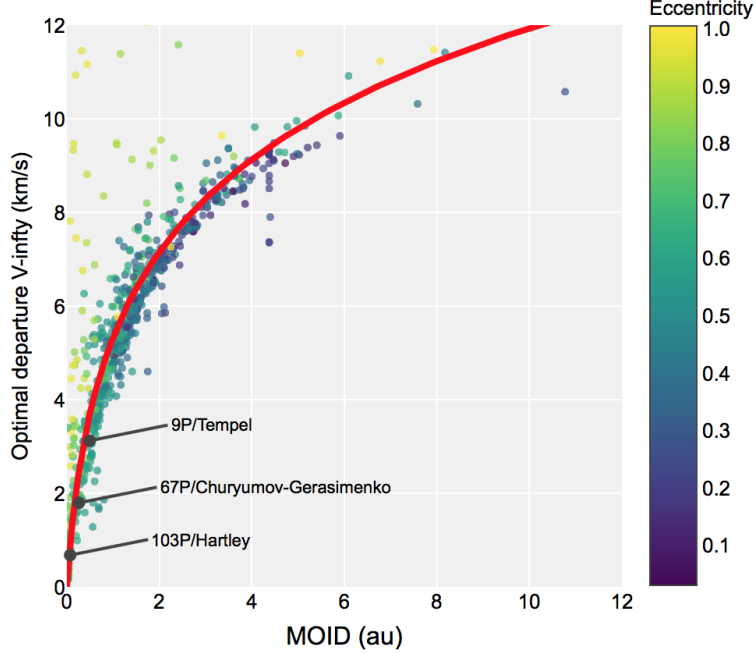


Fig. 10 Distribution of comets by MOID and optimal departure v_∞

of flight decreases the optimal launch date approaches the date of close approach. In fact, the optimal departure C_3 contours form a diagonal straight line with constant arrival date, corresponding to the date of closest approach. This behavior was expected because reaching the asteroid when it is closest to Earth requires the lowest C_3 . There are many launch opportunities that arrive at the date of closest approach, and the optimal one ($v_\infty < 140$ m/s at departure) leaves Earth on August 25, 2028 \pm 2.5 d.

Interestingly, achieving the lowest arrival v_∞ does not correspond to an arrival on the date of closest approach, but rather launching on that date. If the spacecraft is launched when Apophis is closest to Earth, it will be possible to insert the probe in an orbit very similar to that of Apophis, almost matching its orbital elements. A small offset suffices to achieve the encounter and, since the orbits are similar, the incoming v_∞ is low.

The launch-vehicle selection tool described in Sec. B consists in an interactive plot like the one shown in Fig. 12. This figure compares the maximum rendezvous mass that can be launched from Earth using different launch vehicles. Since the relation between the launch mass and the C_3 is different for each launcher, the optimal launch dates and times of flight might not be the same. Although the minimum C_3 is achieved by missions that arrive right at the date of closest approach, the optimal arrival date for a rendezvous mission is actually two years later, on May 20, 2031 \pm 2.5 d. The time of flight of the mission is one year.

VI. Conclusion

The new JPL Small-Body Automatic Mission-Design System provides a database of pre-computed trajectories to all small bodies in the Solar System. By combining this database with the existing Small-Body Database, it is possible to rapidly select potential candidates for preliminary missions. By fitting the mission-design data, we developed approximate analytic expressions that bound the v_∞ that will be required to reach a specific family of small bodies as a function of the minimum orbit intersection distance (MOID). The interactive web interface provides the user with the tools required to explore alternative mission options.

Near-Earth asteroids typically require $C_3 < 10$ km²/s² at departure, which can be achieved with most launch vehicles. Mars-crossing and inner main-belt asteroids exhibit similar expected C_3 values ($C_3 \lesssim 20$ km²/s²), whereas targeting the outer main belt raises the departure characteristic energy requirements to $C_3 > 40$ km²/s². The family of main-belt asteroids is tightly packed in v_∞ -MOID space and the launch requirements have been accurately bounded to $3 < v_\infty < 7$ km/s. Jupiter Trojans also exhibit a rather homogeneous behavior, for which the v_∞ has been constrained to $7 < v_\infty < 9$ km/s. The wide dynamical regime of Centaur orbits leads to different mission requirements, which have

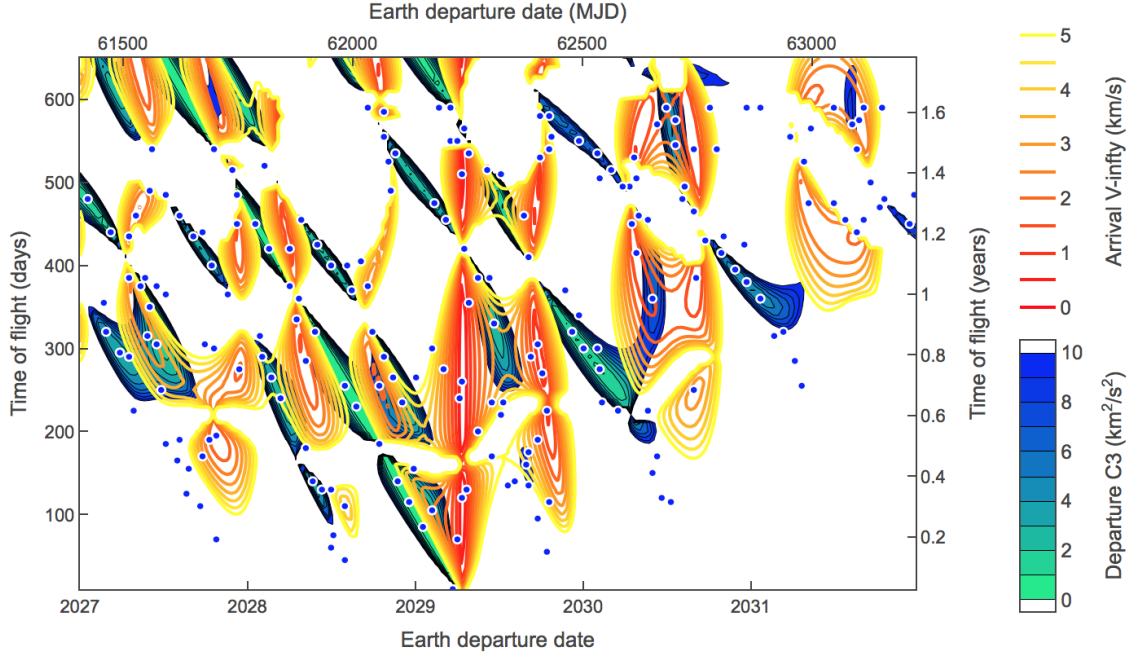


Fig. 11 Transfer map showing missions to asteroid 99942 Apophis

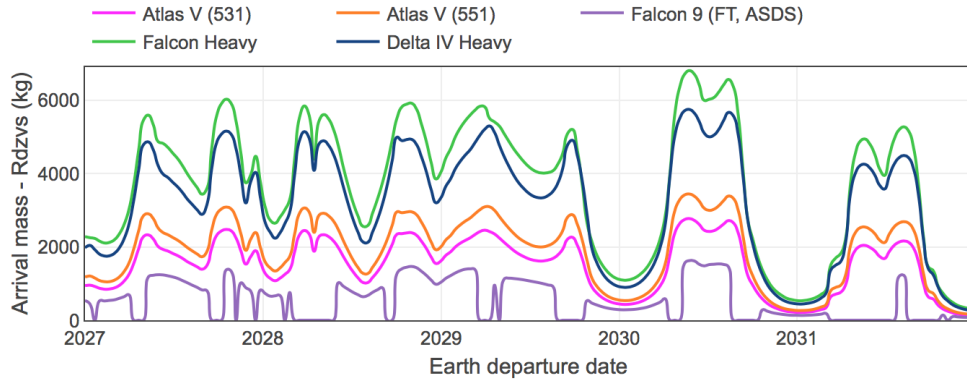


Fig. 12 Maximum rendezvous mass using different launch vehicles (99942 Apophis)

been fitted for rapid evaluation. Although direct impulsive transfers to trans-Neptunian objects are not practical, we found that 23% of these objects can be reached with $C_3 < 150 \text{ km}^2/\text{s}^2$ launching in the next 25 years. Statistics also reveal that 21% of comets can be reached with direct transfers.

The pre-computed missions stored in the database correspond to a time span of 25 years. This is a long period of time for mission-design time scales, but only moderately long or even short when compared to the orbital time scales of the Solar System. Such considerations might question how well will the results presented in the paper apply in the future. For example, 25 years is just a tenth of the period of typical trans-Neptunian objects, and for the case of parabolic and hyperbolic comets the date of perihelion passage plays a crucial role. However, under the assumption that most families are uniformly distributed in terms of their phasing, it is fair to assume that such distributions will average out possible biases when changing the interval of launch dates, and that the statistical conclusions presented here will hold in time.

Appendix

Table 6 presents the optimal mission option (minimum departure v_∞) for the five asteroids and comets with lowest departure v_∞ in each family. The three-letter code for the orbit class is the one introduced in Table 1. Apart from the dates and v_∞ , it includes the range and phase angle at arrival, together with the DLA (departure).

Table 6 Missions to targets with the lowest departure v_{∞}

Designation	Class	Departure date	Arrival date	TOF (d)	$v_{\infty, \text{dep}}$ (km/s)	$v_{\infty, \text{arr}}$ (km/s)	Range (au)	Phase ang. (deg)	DLA (deg)
1998 DK ₃₆	IEO	2031-10-29	2032-02-16	110	0.13	7.46	0.01	99.38	-55.38
481817	IEO	2033-08-14	2034-12-02	475	0.28	13.40	0.19	97.33	-34.89
434326	IEO	2036-12-31	2038-04-10	465	0.46	13.05	0.31	77.36	-16.41
2015 ME ₁₃₁	IEO	2020-01-05	2020-07-28	205	0.52	15.42	0.19	81.25	-19.42
2013 JX ₂₈	IEO	2027-10-10	2028-04-17	190	0.58	12.27	0.23	74.44	-20.79
2014 LY ₂₁	ATE	2019-09-12	2020-06-03	265	0.01	11.79	0.01	61.49	60.58
2008 LD	ATE	2023-03-20	2024-06-02	440	0.03	4.11	0.02	112.13	-48.07
2017 HG ₄	ATE	2041-07-08	2042-04-19	285	0.03	3.73	0.01	127.22	10.46
2005 VL ₁	ATE	2036-08-08	2037-10-27	445	0.04	6.53	0.03	159.05	-10.83
2000 SG ₃₄₄	ATE	2027-08-01	2028-05-12	285	0.04	1.49	0.02	167.34	-40.76
2016 EO ₂₈	APO	2033-01-31	2035-03-02	760	0.01	6.99	0.03	156.73	-47.50
443104	APO	2029-11-08	2031-06-21	590	0.01	6.94	0.01	148.88	74.12
2011 CF ₂₂	APO	2037-04-10	2041-02-08	1400	0.01	19.11	0.03	176.67	32.65
2003 DW ₁₀	APO	2040-07-08	2043-03-05	970	0.02	7.84	0.05	29.27	-23.77
2014 HB ₁₇₇	APO	2033-12-27	2034-05-06	130	0.02	6.43	0.00	19.36	-34.91
2010 FD	AMO	2029-06-26	2034-03-02	1710	0.03	9.70	0.12	56.19	-17.29
2014 SC	AMO	2041-05-29	2044-09-30	1220	0.07	8.13	0.13	75.20	-51.76
2013 ML ₃	AMO	2037-09-07	2042-06-18	1745	0.10	9.17	0.27	81.37	63.09
2009 FS ₄	AMO	2031-07-26	2032-03-27	245	0.11	9.08	0.01	55.66	73.54
2012 LT	AMO	2021-10-06	2026-07-02	1730	0.12	8.34	0.38	75.65	50.07
2014 HS ₁₉₅	MCA	2028-09-13	2029-05-11	240	1.59	9.76	0.82	124.77	14.05
2005 RD ₁	MCA	2041-11-29	2043-11-14	715	1.76	9.14	2.04	92.19	-3.84
2007 MK ₂₄	MCA	2025-12-18	2029-01-21	1130	1.80	7.37	2.23	102.10	8.27
2014 PL ₅₀	MCA	2018-02-08	2021-03-04	1120	1.85	9.13	2.23	92.07	-17.69
2015 KC ₂₃	MCA	2027-12-13	2028-07-10	210	1.85	7.00	0.75	91.11	3.79
2010 DS ₂₆	IMB	2033-01-25	2035-05-30	855	3.46	9.57	1.52	93.13	-17.02
15374	IMB	2027-01-25	2029-06-08	865	3.48	13.30	1.37	91.97	-12.22
2010 EP ₁₉	IMB	2042-01-28	2044-04-27	820	3.48	9.30	1.82	83.38	-14.99
2010 EV ₁₄₆	IMB	2040-01-19	2040-11-24	310	3.48	7.66	2.27	95.41	-5.23
2017 BR ₉₁	IMB	2042-01-23	2042-10-10	260	3.49	8.09	1.84	78.37	-16.09
2014 SH ₁	MBA	2031-01-31	2033-04-20	810	3.37	7.64	1.97	78.71	-9.74
2010 HS ₂₂	MBA	2023-01-13	2026-10-09	1365	3.39	12.46	1.98	86.64	-11.93
137253	MBA	2032-12-09	2036-10-19	1410	3.42	6.25	2.33	95.36	1.52
2013 LL ₁₄	MBA	2039-01-29	2042-12-09	1410	3.42	9.47	2.37	90.09	-15.14
2009 QK ₆₁	MBA	2041-01-03	2041-10-20	290	3.42	7.27	2.06	100.83	-14.05
2012 TA ₅₃	OMB	2040-02-23	2043-02-12	1085	1.08	10.77	1.87	109.30	-15.84
2016 QH ₁₀	OMB	2037-03-20	2041-01-03	1385	1.12	13.94	2.03	96.35	-2.79
2016 BZ ₁₃	OMB	2042-04-08	2046-12-13	1710	1.23	11.34	0.86	99.56	32.58
2000 XO ₈	OMB	2042-04-18	2044-03-13	695	1.75	13.03	1.93	124.40	1.55
2013 TG ₆₉	OMB	2038-02-18	2043-12-09	2120	1.99	9.99	1.32	57.89	-21.21

Table 6 (cont.) Missions to targets with the lowest departure v_{∞}

Designation	Class	Departure date	Arrival date	TOF (d)	$v_{\infty, \text{dep}}$ (km/s)	$v_{\infty, \text{arr}}$ (km/s)	Range (au)	Phase ang. (deg)	DLA (deg)
2011 WA ₂₄	TJN	2036-05-30	2045-01-13	3150	6.20	8.26	1.67	115.42	-18.96
2010 KF ₉₈	TJN	2026-01-18	2027-06-22	520	6.81	10.43	2.24	85.94	-4.34
2013 BX ₄₄	TJN	2028-11-28	2037-04-10	3055	7.23	8.34	2.92	92.92	6.04
2010 OG ₈₃	TJN	2041-11-10	2043-09-06	665	7.29	9.10	3.88	99.21	15.58
2013 BL ₂₇	TJN	2036-03-16	2041-02-28	1810	7.29	8.57	4.43	89.39	-22.42
2010 LG ₆₁	CEN	2023-01-02	2029-01-03	2193	2.59	51.65	2.24	94.59	12.50
5335	CEN	2024-07-11	2031-08-01	2577	3.70	28.28	2.60	90.24	23.92
2015 VH ₁₀₅	CEN	2022-02-25	2029-05-10	2631	3.97	19.06	2.04	49.76	-35.52
2017 AR ₂₀	CEN	2026-08-14	2032-07-13	2160	4.04	16.43	2.58	141.20	18.50
2014 KG ₂	CEN	2042-02-07	2048-08-04	2370	4.50	20.78	1.11	144.52	-4.02
2002 PR ₁₇₀	TNO	2027-06-08	2039-09-10	4477	11.13	9.00	11.53	109.92	-14.92
2016 FL ₅₉	TNO	2025-12-24	2045-07-31	7159	11.21	7.32	19.63	94.57	-0.88
2013 EH ₁₅₄	TNO	2022-12-22	2044-01-02	7681	11.40	4.95	26.57	79.93	-0.17
469442	TNO	2022-04-22	2042-09-01	7437	11.44	6.37	20.74	132.43	-19.02
2014 WV ₅₀₈	TNO	2017-11-06	2031-05-13	4936	11.45	5.63	20.34	102.98	17.71
55P	HTC	2026-12-31	2031-05-29	1610	1.37	70.46	1.97	92.46	35.24
2012 NJ	HTC	2030-12-19	2037-02-17	2252	2.61	40.70	2.31	104.02	-24.61
161P	HTC	2042-02-24	2047-02-20	1822	2.74	42.02	2.33	77.81	-11.43
2010 L ₅	HTC	2030-01-20	2033-11-03	1383	2.82	74.75	0.34	78.50	39.87
1991 L ₃	HTC	2035-10-27	2042-09-29	2529	2.99	15.51	0.62	61.17	8.26
332P-G	ETc	2021-09-08	2027-01-20	1960	3.37	10.19	1.48	123.70	24.92
332P-D	ETc	2025-09-22	2032-08-01	2505	3.44	9.76	2.37	118.54	20.48
332P-H	ETc	2025-09-17	2032-08-11	2520	3.45	9.87	2.46	120.24	22.17
332P-I	ETc	2028-09-16	2032-08-01	1415	3.48	9.90	2.37	122.00	27.43
332P	ETc	2025-09-17	2032-07-27	2505	3.48	9.79	2.33	117.08	14.56
73P-U	JFc	2018-08-25	2022-05-06	1350	0.17	12.28	0.43	61.38	-8.35
73P-R	JFc	2029-08-27	2033-04-23	1335	0.18	13.62	0.28	36.99	-72.16
73P-Z	JFc	2028-08-02	2033-04-23	1725	0.19	13.76	0.25	35.22	-64.69
73P-M	JFc	2028-08-07	2033-04-18	1715	0.19	13.69	0.36	36.80	-71.63
73P-K	JFc	2028-10-01	2033-04-08	1650	0.20	13.33	0.58	39.42	-22.86
2015 M ₂	CTc	2022-12-16	2033-05-12	3800	9.19	6.57	5.42	81.96	2.19
2005 T ₃	CTc	2036-04-18	2047-01-06	3915	9.39	6.70	6.11	96.12	-21.80
2005 S ₂	CTc	2038-03-06	2049-05-19	4092	9.43	6.72	6.99	73.12	-23.27
39P	CTc	2022-07-07	2026-01-29	1302	9.48	6.40	5.35	107.70	4.33
2011 S ₁	CTc	2027-05-01	2039-03-30	4351	9.63	6.69	7.78	88.81	-17.92
2016 R ₂	COM	2018-01-02	2032-12-03	5449	12.06	2.06	31.91	114.53	-1.50
2009 B ₂	COM	2018-04-22	2058-02-21	14550	12.22	2.21	58.34	53.90	-18.21

Table 6 (cont.) Missions to targets with the lowest departure v_{∞}

Designation	Class	Departure date	Arrival date	TOF (d)	$v_{\infty,dep}$ (km/s)	$v_{\infty,arr}$ (km/s)	Range (au)	Phase ang. (deg)	DLA (deg)
2017 K ₅	PAR	2018-02-01	2020-08-04	915	10.67	17.00	6.86	64.65	-17.22
2017 M ₅	PAR	2018-05-22	2022-05-31	1470	11.40	5.84	12.01	98.81	-9.69
2017 K ₂	HYP	2018-11-23	2022-08-24	1370	5.77	29.76	2.06	72.75	0.80
2017 M ₄	HYP	2017-12-13	2019-03-08	450	7.26	28.10	3.24	87.30	11.97
2017 B ₃	HYP	2018-04-12	2020-09-13	885	9.64	12.20	5.27	116.49	-22.62
2016 Q ₂	HYP	2018-08-20	2027-11-26	3385	11.23	10.05	15.52	123.29	19.66
2010 U ₃	HYP	2018-11-18	2026-11-21	2925	11.48	6.25	18.40	106.25	12.18

Acknowledgments

This research was carried out at the Jet Propulsion Laboratory, California Institute of Technology, under a contract with the National Aeronautics and Space Administration. We thank Nitin Arora for providing the Lambert solver, and for his feedback on different stages of the project.

References

- [1] Shoemaker, E., and Helin, E., "Earth-approaching asteroids as targets for exploration," Report N78-29022, California Institute of Technology, Jan. 1978.
- [2] Barbee, B. W., Esposito, T., Pinon III, E., Hur-Diaz, S., Mink, R. G., and Adamo, D. R., "A comprehensive ongoing survey of the near-Earth asteroid population for human mission accessibility," *Proceedings of the AIAA/AAS Guidance, Navigation, and Control Conference, (Toronto, Ontario, Canada)*, 2010, pp. 2-5.
- [3] Brophy, J. R., Gershman, R., Strange, N., Landau, D., Merrill, R. G., and Kerlake, T., "300-kW solar electric propulsion system configuration for human exploration of near-Earth asteroids," *AIAA Paper*, Vol. 5514, 2011, p. 2011.
- [4] Landau, D., and Strange, N., "Near-Earth asteroids accessible to human exploration with high-power electric propulsion," *AAS/AIAA astrodynamics specialist conference*, Vol. 11, 2011.
- [5] Barbee, B. W., Abell, P. A., Adamo, D. R., Mazanek, D. D., Johnson, L. N., Yeomans, D. K., Chodas, P. W., Chamberlin, A. B., Benner, L. A., Taylor, P., et al., "The Mission Accessibility of Near-Earth Asteroids," *4th IAA Planetary Defense Conference - PDC 2015*, Frascati, Roma, Italy, 2015.
- [6] Perozzi, E., Rossi, A., and Valsecchi, G. B., "Basic targeting strategies for rendezvous and flyby missions to the near-Earth asteroids," *Planet. Space Sci.*, Vol. 49, No. 1, 2001, pp. 3-22.
- [7] Edelbaum, T. N., "Optimum power-limited orbit transfer in strong gravity fields," *AIAA J.*, Vol. 3, No. 5, 1965, pp. 921-925. doi:10.2514/3.3016.
- [8] Arora, N., and Russell, R. P., "A fast and robust multiple revolution Lambert algorithm using a cosine transformation," *2013 AAS/AIAA Astrodynamics Specialist Conference*, 2013, No. AAS13-728.
- [9] Bottke, W. F., Durda, D. D., Nesvorný, D., Jedicke, R., Morbidelli, A., Vokrouhlický, D., and Levison, H. F., "Linking the collisional history of the main asteroid belt to its dynamical excitation and depletion," *Icarus*, Vol. 179, No. 1, 2005, pp. 63-94. doi:10.1016/j.icarus.2005.05.017.
- [10] Horner, J., Evans, N., and Bailey, M. E., "Simulations of the population of Centaurs-I. The bulk statistics," *Mon. Not. R. Astron. Soc.*, Vol. 354, No. 3, 2004, pp. 798-810. doi:10.1111/j.1365-2966.2004.08240.x.
- [11] Oort, J. H., et al., "The structure of the cloud of comets surrounding the Solar System and a hypothesis concerning its origin," *Bull. Astron. Inst. Neth.*, Vol. 11, 1950, p. 91.
- [12] Duncan, M., Quinn, T., and Tremaine, S., "The origin of short-period comets," *Astrophys. J.*, Vol. 328, 1988, pp. L69-L73.
- [13] Blume, W. H., "Deep Impact mission design," *Space Sci. Rev.*, Vol. 117, 2005, pp. 23-42. doi:10.1007/s11214-005-3386-4.
- [14] Chesley, S. R., "Potential impact detection for Near-Earth asteroids: the case of 99942 Apophis (2004 MN 4)," *Proc. Int. Astron. Union*, Vol. 1, No. S229, 2005, pp. 215-228. doi:10.1017/S1743921305006769.